BIOCHEMISTRY
including biophysical chemistry & molecular biology

Article

pubs.acs.org/biochemistry

GTP Binding Leads to Narrowing of the Conformer Population While Preserving the Structure of the RNA Aptamer: A Site-Specific Time-Resolved Fluorescence Dynamics Study

T. Sanjoy Singh,[†,§] B. J. Rao,*[,‡] and G. Krishnamoorthy*[,†]

[†]Department of Chemical Sciences and [‡]Department of Biological Sciences, Tata Institute of Fundamental Research, Homi Bhabha Road, Mumbai 400 005, India

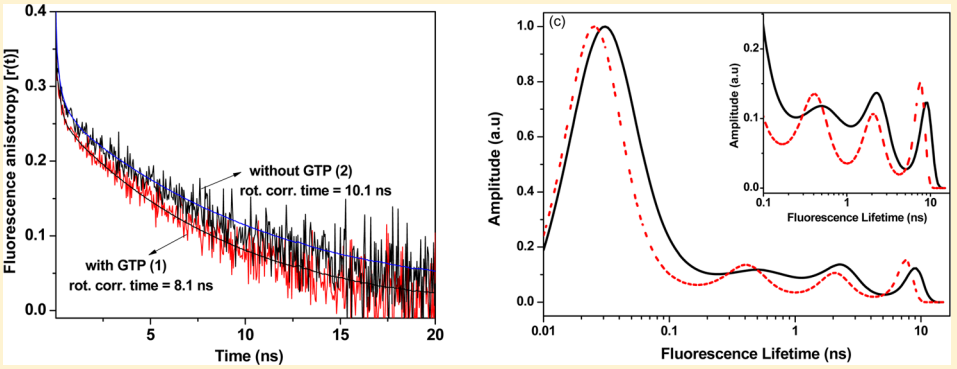

ABSTRACT: In this study, we employed a combination of steady-state and time-resolved fluorescence spectroscopy and studied the site-specific dynamics in a GTP aptamer using 2-aminopurine as a fluorescent probe. We compared the dynamics of the GTP-bound aptamer with that of the free aptamer as well as when it is denatured. GTP binding leads to an overall compaction of structure in the aptamer. The general pattern of fluorescence lifetimes and correlation times scanned across several locations in the aptamer does not seem to change following GTP binding. However, a remarkable narrowing of the lifetime distribution of the aptamer ensues following its compaction by GTP binding. Interestingly, such a "conformational narrowing" is evident from the lifetime readouts of the nucleotide belonging to the stem as well as the "bulge" part of the aptamer, independent of whether it is directly interacting with GTP. Taken together, these results underscore the importance of an overall intrinsic structure associated with the free aptamer that is further modulated following GTP binding. This work provides strong support for the "conformational selection" hypothesis of ligand binding.

RNA aptamers are RNA oligonucleotides that can bind specifically to a wide range of target molecules such as small molecules, cofactors, amino acids, etc., with high affinity.[1−3] Aptamers are selected from a combinatorial library through an artificial evolution procedure called systematic evolution of ligands by exponential enrichment (SELEX).[4,5] There has been an exponentially growing number of applications of aptamers, namely, as biosensors,[6,7] as a tool for metabolite sensing,[8] as diagnostics or biomedical applications,[9] and as drug delivery tools.[10] One of the main attractive properties of aptamers is the in vitro selection procedure that can provide an aptamer against virtually any target of choice and with a predefined affinity. The structural flexibility of oligonucleotides allows for adaptation of the aptamer to various structures.[1,11−20] The recognition and binding of a small molecule ligand by nucleic acids are thought to be based mainly on stacking interactions and hydrogen bonding.[18,21,22] These types of interactions are crucial for RNA function in nature as well as in the context of RNA as a drug target.[23,24] RNA aptamers are ideal systems for detailed studies of these interactions.[25] Several structures of aptamer (both artificial and natural)−ligand complexes have been determined using X-ray crystallography[26−30] and nuclear magnetic resonance (NMR) spectroscopy.[14−23,31−37] The structures of complexes of aptamers with ATP, biotin, or FMN, among others, demonstrated that specificity is most often achieved by specific hydrogen bonding patterns and stacking of aromatic ring systems in the ligand with bases in the RNA.[21,31,38] Another characteristic feature of these complexes, especially those with artificially selected aptamers, is the fact that the RNA binding pocket in its ligand free form is largely unstructured and folding occurs simultaneously with ligand binding, a process that has been termed conformational selection or adaptive binding.[19,22,39,40]

Artificially selected RNA aptamers are quite small in size, very similar to the aptamer domain of RNA switches.[28−37,41,42] In RNA switches, structural changes in the aptamer domain caused by ligand binding led to the switching action. Understanding the intricacies of ligand-induced changes in

Received: August 16, 2012
Revised: October 19, 2012
Published: October 30, 2012

structure and dynamics in artificial RNA aptamers could, in principle, shed light on the mechanism of the function of RNA switches. Significantly smaller RNA aptamers when compared to RNA switches make the aptamers easy to study structurally as model systems.[1] Furthermore, there is a lack of structural information about free artificial aptamers presumably because of their dynamic nature.[1,14,18,19] Information about ligand-induced changes in the structure and dynamics of aptamers is expected to offer insights into the resolution of the mechanism of recognition, viz., "conformation capture" versus "induced fit".[39,40]

In this work, we have studied site-specific dynamics of the class I GTP aptamer (Figure 1) and the changes induced by the

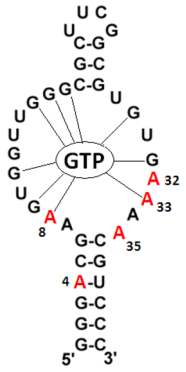

Figure 1. Secondary structure model of the GTP-binding RNA aptamer.[14] Adenines (A) colored red are 2-AP, singly incorporated in each aptamer.

binding of GTP using the fluorescent analogue of adenine, 2-aminopurine (2-AP)[43,44] located at specific positions in the aptamer sequence. 2-AP has been very effectively used to study both specific and nonspecific aspects of the structure and dynamics of the nucleic acids in a wide variety of situations.[45−49] We have used dynamic fluorescence parameters such as the excited-state lifetime and rotational depolarization time of 2-AP to infer dynamics of the RNA aptamer. We find that the binding of GTP leads to site-specific changes in the structure and dynamics of the aptamer. Our results are largely in line with the conformational selection[18] and adaptive recognition[1,39,40] hypotheses but also underscore the importance of preexisting structural features in the free aptamer that eventually lead to adaptive recognition of the ligand. One of the key tenets of the "conformational selection" model, namely, that the ligand-bound conformation preexists in the population of the free aptamer, is met in this study. More specifically, we observe a narrowing of the conformational heterogeneity in the aptamer, resulting in an overall compaction of the structure following GTP binding. This result reflects a scenario consistent with weakly populated conformations responsible for recognition and binding of the ligand to an aptamer with a subsequent population shift toward these "bound-form conformers".

MATERIALS AND METHODS

Materials. Oligonucleotides containing 2-aminopurine (2-AP) were purchased from Fidelity Systems Inc. The oligonucleotides were purified on denaturing polyacrylamide gels and desalted by the supplier. RNA was quantified by measuring the absorbance at 260 nm, which was expressed as the total nucleotide concentration. The oligonucleotides with different 2-AP positions used for the experiment are described in Figure 1. PicoGreen (PG) was of the highest available purity from Molecular Probes Inc. and used without further purification. The PG concentration was 0.12 μM. Guanosine 5-triphosphate (GTP) was of the highest available purity from Roche Applied Sciences. The buffer used in all the experiments consisted of 10 mM Tris-HCl (pH 7.5), 5 mM magnesium chloride ($MgCl_2$), and 150 mM potassium chloride (KCl). Acrylamide and urea were purchased from USB Corp. and used without further purification. The concentration of the urea stock solution (~7 M) was determined by the refractive index measurement.

Sample Preparation. The RNA sample in 10 mM Tris-HCl (pH 7.5), 5 mM $MgCl_2$, and 150 mM KCl were heated to 90−95 °C for 2 min and then slowly cooled to room temperature over a period of 12−14 h.[50] Measurements were taken at room temperature (24 ± 1 °C) unless mentioned otherwise. RNA concentrations were in the range of 6−15 μM, and the ligand concentration is much higher, on the order of 100 μM, which is also much higher than the reported dissociation constant (k_d ~ 75 nM) of the RNA aptamer.[2] To ensure that all the RNA molecules are bound to GTP, the mean fluorescence lifetimes of some of the RNA samples were titrated with GTP in the concentration range of 0−400 μM. It was found that the observed change in the mean lifetime (see below) saturated at <100 μM GTP (data not shown). All experiments were conducted by maintaining the conditions under which RNA was not subject to any spurious degradation by ubiquitous RNases present. We monitored the quality of RNA before and after each experiment. No degradation of RNA was observed.

Fluorescence Measurement. *Steady-State Fluorescence Spectroscopy.* Steady-state fluorescence spectra were recorded using a Horiba Jobin Yvon Fluorolog-3 spectrofluorometer. All the fluorescence spectra were corrected for the spectral sensitivity of the photomultiplier. The bandwidth used was between 1.5 and 5 nm. Appropriate filters were used before the emission monochromator to prevent the excitation light from entering it.

Time-Resolved Fluorescence Spectroscopy. The time-resolved fluorescence intensity and anisotropy decay of 2-AP were measured by employing a CW passively mode-locked frequency-doubled Nd:YAG laser (Vanguard, Spectra Physics) driven rhodamine 6G dye laser that generates pulses with a width of 1 ps. 2-AP in RNA was excited by using the second harmonic output (305 nm) of an angle-tuned KDP crystal. Fluorescence decay curves were obtained by using a time-correlated single-photon counting (TCSPC) setup, coupled to a microchannel plate photomultiplier (model 2809U, Hamamatsu Corp.). The instrument response function (IRF) was obtained at 305 nm using a dilute colloidal suspension of dried nondairy coffee whitener. The half-width of the IRF was ~40 ps. The time per channel was ~39.2 ps. The samples were excited at 305 nm, and the fluorescence emission was collected through a 345 nm cutoff filter followed by a monochromator at 370 nm with a collection bandwidth of 3 nm. The cutoff filter was used to prevent scattering of the excitation beam from the sample. The number of counts in the peak channel was at least 10000. In fluorescence lifetime measurements, the emission was monitored at the magic angle (54.7°) to eliminate the contribution from the decay of anisotropy. In time-resolved anisotropy measurements, the emission was collected at

dx.doi.org/10.1021/bi301110u | *Biochemistry* 2012, 51, 9260−9269

directions parallel (||) and perpendicular (⊥) to the polarization of the excitation beam.

The experimentally obtained fluorescence decay traces, $I(t)$, were analyzed by the nonlinear least-squares iterative deconvolution method based on the Levenberg–Marquardt algorithm[51] and expressed as a sum of exponentials with the equation

$$I(t) = \sum_i \alpha_i \exp(-t/\tau_i) \quad (1)$$

where α_i is the amplitude of the ith component associated with fluorescence lifetime τ_i such that $\sum\alpha_i = 1$. The mean lifetime τ_m ($=\sum_i\alpha_i\tau_i$) gives us information about the average fluorescence yield of the system.

The time-resolved fluorescence anisotropy decay curves were obtained by measuring the fluorescence emission intensity at parallel $\|(t)$ and perpendicular $\perp(t)$ directions to the polarization of the excitation beam and constructing the time-dependent anisotropy, $r(t)$, with the following equation:

$$r(t) = \frac{I_{\|}(t) - G(\lambda)I_{\perp}(t)}{I_{\perp}(t) + 2G(\lambda)I_{\perp}(t)} \quad (2)$$

where $G(\lambda)$ is the geometry factor at wavelength of emission λ. The magnitude of the geometry factor for the emission collection optics was determined independently using a standard solution of 2-AP for which the fluorescence lifetime is 11.3 ns.

Time-resolved anisotropy decays were analyzed with the following sets of equations:

$$I_{\|}(t) = \frac{1}{3}I(t)[1 + 2r(t)] \quad (3)$$

$$I_{\perp}(t) = \frac{1}{3}I(t)[1 - r(t)] \quad (4)$$

$$r(t) = r_0[\beta_1 \exp(-\tau/\phi_1) + \beta_2 \exp(-\tau/\phi_2)] \quad (5)$$

where r_0 is the initial anisotropy and β_i is the amplitude of the ith rotational correlation time (ϕ_i) such that $\sum\beta_i = 1$. These parameters were obtained by deconvoluting the decays with IRF, and the initial anisotropy ($r_0 = 0.31$) estimated in a separate experiment on 2-AP in 50% glycerol was kept fixed during the analysis. The goodness of the fits was checked by both the reduced χ^2 value and randomness of residuals.

Fluorescence Quenching. The solvent accessibility of 2-AP residues was monitored by collisional quenching with acrylamide. A titration stock was made with ~5 M acrylamide, 10 mM Tris-HCl (pH 7.5), 150 mM KCl, and 5 mM $MgCl_2$, and the acrylamide was added over the concentration range of 0–200 mM. Fluorescence lifetimes were measured immediately after mixing, and acrylamide quenching titrations were fit to the Stern–Volmer equation[52] for analysis of collisional quenching:

$$\tau_0/\tau = 1 + k_q\tau_0[Q] \quad (6)$$

where τ_0 and τ are the lifetimes in the absence and presence of the quencher, respectively, [Q] is the acrylamide concentration, and k_q is the bimolecular quenching rate constant (M^{-1} s^{-1}).

Maximum Entropy Method of Analysis (MEM). The lifetime distributions of the GTP binding RNA aptamer in the presence and absence of GTP were obtained by analyzing the fluorescence decay kinetics of 2-AP using MEM analysis.[53,54] For estimating lifetime distributions, the method based on maximum entropy analysis that provides a model free approach was employed. Maximum entropy method (MEM) analysis does not make any assumption about the shape of the distribution, unlike other methods that assume the distribution function (Gaussian or Lorentzian) and the number of peaks prior to analysis.[55]

MEM analysis treats the fluorescence decay as arising from a distribution of a large number (~100–150) of discrete lifetime values equally spaced in the log(τ) space covering the range from 10 ps to 20 ns or over a similar range depending on the nature of the fluorescent molecule. The analysis begins by assigning equal probability (amplitude) to all the lifetime values. Subsequently, in each iteration during the analysis, the distribution is modified leading to minimization of χ^2 and maximization of the Shannon–Jaynes entropy function

$$S = -\sum \alpha_i \log \alpha_i \quad (7)$$

where α_i is the probability (amplitude) of the ith lifetime. If many possible distributions have the same value or a similar value of χ^2, then the maximum entropy criterion selects the distribution for which entropy (S) is maximal. Thus, MEM analysis results in a lifetime distribution that is independent of any mathematical model. The values of χ^2 were in the range of 1.0–1.05 for all the MEM analyses.

UV Melting. UV melting experiments were conducted on a UV–visible spectrophotometer (PerkinElmer, Lambda-750) equipped with Peltier temperature control elements within the temperature range of 20–92 °C using a quartz cuvette with a 1 mm path length according to established procedures.[56] RNA samples were in 10 mM Tris-HCl (pH 7.5), 5 mM $MgCl_2$, and 150 mM KCl at final concentrations of 6–15 μM. The melting profiles were measured at a wavelength of 260 nm, and data were collected with heating rates of 1 °C/min, where RNA samples were sealed in the cuvette during the experiment to prevent their evaporation while they were being heated.

RESULTS AND DISCUSSION

GTP-Induced Structural Changes. *Melting Transition.* The melting profile of the RNA aptamer (Figure 1) was monitored by measuring absorption at 260 nm in the presence and absence of ligand in the temperature range of 20–92 °C (Figure 2). The melting curves show two transitions in the free aptamer. The two transitions could be assigned to the premelting and the overall melting of the aptamer. The premelting transition in nucleic acid structures is generally

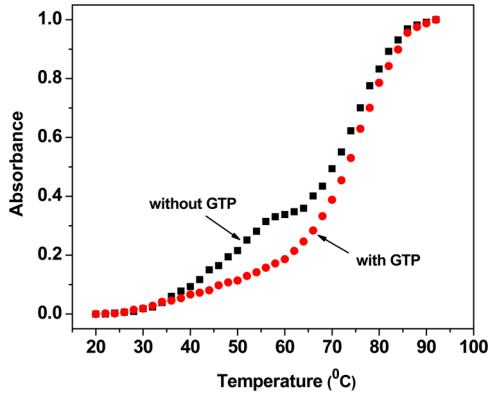

Figure 2. UV melting profile of the GTP-binding RNA aptamer in the presence (●) and absence (■) of ligand.

dx.doi.org/10.1021/bi301110u | *Biochemistry* 2012, 51, 9260–9269

ascribed to local events, and conformational fluctuations and the dynamics of this transition are associated with function.[57] In the presence of GTP, the melting curve shows a single transition similar to the second transition observed in the absence of GTP and no premelting transition was evident (Figure 2). The main transition observed in the presence or absence of GTP showed a gradual increase in absorbance until a plateau was reached above 90 °C. This result indicated the structural difference in the GTP-bound aptamer where ligand binding caused a reduction in the level of conformational fluctuation and stabilized the aptamer as evidenced by the abolishment of pretransition melting.

Fluorescence Anisotropy Decay Kinetics of PicoGreen Shows GTP-Induced Compaction. PicoGreen (PG), an unsymmetric monomethine cyanine dye, has been used in interesting applications in scoring dynamics of nucleic acids.[58,59] It binds to both single- and double-stranded nucleic acids by a variety of binding modes.[60] We used PG to estimate the overall hydrodynamic size of the aptamer from the fluorescence anisotropy decay kinetics of the PG−aptamer complex. The fluorescence anisotropy decay of PG in both the free and GTP-bound aptamer (Figure 3) could be fit

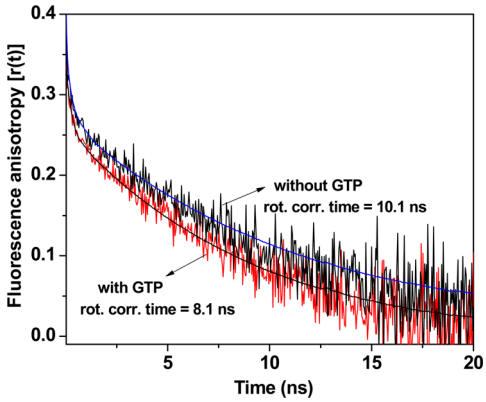

Figure 3. Hydrodynamic size of the GTP aptamer monitored by the fluorescence depolarization kinetics of PicoGreen. The corresponding rotational correlation times (ϕ) in the presence and absence of a ligand are shown.

satisfactorily to a sum of two exponentials (eq 5). The two rotational correlation times (ϕ) could be interpreted as being due to internal motion of the fluorophore (ϕ_1) and the global tumbling motion (ϕ_2) of the aptamer. The global tumbling motion (ϕ_2) gives an estimate of the effective hydrodynamic size through the Stokes−Einstein relationship $\phi = \eta V/kT$, where η, V, k, and T represent the viscosity, molecular volume, Boltzmann constant, and temperature, respectively. The values of ϕ_2 for the anisotropy decay curves were 10.1 ± 0.5 and 8.1 ± 0.5 ns for the free aptamer and the aptamer−GTP complex, respectively. The GTP binding-induced decrease in the value of ϕ_2 is an indication that the overall size of the aptamer decreases, thereby implying a structural compaction following GTP binding. This observation is consistent with the GTP-induced abolition of the premelting transition observed in melting studies (Figure 2) that was probably caused by inhibition of conformational fluctuation.

Site-Specific Changes in Dynamics Probed by 2-Aminopurine. We studied both the steady-state and time-resolved fluorescence of 2-AP incorporated at various locations of adenine in the aptamer, one at a time (Figure 1), to investigate the changes in local structure and dynamics caused by the binding of GTP. 2-AP can be selectively excited even in the presence of proteins because of its long (315 nm) wavelength absorption. Furthermore, the fluorescence intensity of 2-AP is quite sensitive to stacking interactions with neighboring bases as well as to dynamics of near neighbors.[47,61−64]

Site-Specific Fluorescence Decay Kinetics. Free 2-AP in aqueous solutions has a fluorescence quantum yield of 0.68[65] and has a single fluorescence lifetime of 11.3 ns. When 2-AP is incorporated into polynucleotides, its photophysics becomes extremely complex, leading to multiexponential decays with time constants ranging from 50 ps to ∼10 ns.[65−67] This heterogeneity is usually interpreted as being caused by the distribution of partially stacked structures with varying dynamics. While the shortest lifetime component has been used to derive information about the level of duplex formation,[66] the longest component (8−10 ns) is generally assigned to conformations in which 2-AP is either extrahelical or unstacked in the nucleic acid helix.[65] The heterogeneity of population observed through fluorescence lifetimes is generally not seen from other measurements such as NMR, CD, etc., probably because of averaging of various conformers. The rapid time scale associated with fluorescence decay kinetics, in comparison with the slower time scales in NMR, allows the visualization of various conformers as a snapshot picture.

Picosecond time-resolved fluorescence intensity decay kinetics of 2-AP in the free and GTP-bound RNA aptamer showed the presence of at least four lifetime components (Table 1) as observed earlier in the case of DNA oligonucleotides.[46,68] Prior to examination of the individual lifetime components, it is very instructive to focus attention on the profile of the mean lifetime (τ_m) measured at various locations in the aptamer (Table 1). The mean fluorescence lifetime (τ_m) of 2-AP is very sensitive to its environment in polynucleotides,[46,61−64] and hence, the observed position dependence in the GTP aptamer (Table 2 and Figure 4A) is clearly indicative of a structured RNA. As expected, 2-AP located at the fourth position (Figure 1), which is part of a stem (duplex), showed the lowest τ_m compared to the rest. It is also striking to note that the pattern of variation in τ_m vis-à-vis the location of 2-AP is largely preserved in the aptamer, independent of whether it was GTP-bound. This result has important implications in the context of the mechanism of ligand binding and earlier solution NMR structural studies of aptamer−ligand complexes.[14−19] It indicates that the three-dimensional structure is largely similar in both the free aptamer and the aptamer−GTP complex. This conclusion may seem contradictory to that derived from NMR studies on several artificially selected aptamers.[14−19] These structural studies have emphasized the highly flexible structure of free aptamers leading to the absence of dispersion in NMR resonances that becomes sharp and dispersed upon ligand binding.[14−19] It is likely that although the free aptamer could be conformationally heterogeneous compared to the complex, its average structure is perhaps largely similar to that of the complex, a conclusion that was not evident through these early NMR studies. Recent NMR studies of aptamer segments of riboswitches, however, have indeed shown preorganization of the aptamer domain into "bound" structure even in the absence of the ligand.[33,34] It is noteworthy that the relative populations of these conformers vary over a wide range from one riboswitch to another.[28−37]

The individual lifetime component also has interesting information to offer about the structure of the aptamer and

dx.doi.org/10.1021/bi301110u | *Biochemistry* 2012, 51, 9260−9269

Table 1. Parameters Associated with Fluorescence Intensity Decay in the GTP-Binding RNA Aptamer

sample[a]	τ_1 (α_1)	τ_2 (α_2)	τ_3 (α_3)	τ_4 (α_4)	τ_m (ns)	χ^2
Without GTP: Fluorescence Lifetimes in ns (amplitude)						
GTP(4)	0.03 (0.85)	0.44 (0.07)	2.21 (0.04)	8.01 (0.02)	0.35	1.01
GTP(8)	0.09 (0.45)	0.59 (0.19)	2.97 (0.15)	8.71 (0.20)	2.38	1.00
GTP(32)	0.15 (0.32)	0.74 (0.18)	3.11 (0.25)	8.46 (0.25)	2.98	1.03
GTP(33)	0.29 (0.32)	0.72 (0.19)	2.60 (0.28)	7.51 (0.19)	2.46	1.03
GTP(35)	0.19 (0.48)	0.79 (0.20)	2.97 (0.18)	8.18 (0.13)	1.83	1.01
With GTP: Fluorescence Lifetimes in ns (amplitude)						
GTP(4)	0.02 (0.86)	0.33 (0.07)	2.12 (0.04)	7.44 (0.02)	0.30	1.08
GTP(8)	0.09 (0.57)	0.59 (0.19)	2.82 (0.12)	8.55 (0.11)	1.41	1.01
GTP(32)	0.12 (0.37)	0.87 (0.20)	3.24 (0.22)	8.43 (0.20)	2.65	1.11
GTP(33)	0.08 (0.39)	0.46 (0.23)	2.44 (0.23)	7.58 (0.14)	1.81	1.04
GTP(35)	0.10 (0.39)	0.54 (0.26)	2.42 (0.18)	7.29 (0.15)	1.73	1.01
With Urea (without GTP): Fluorescence Lifetimes in ns (amplitude)						
GTP(4)	0.05 (0.44)	0.34 (0.16)	1.78 (0.16)	5.15 (0.22)	1.52	1.00
GTP(8)	0.23 (0.33)	1.11 (0.24)	3.75 (0.24)	8.12 (0.19)	2.79	1.01
GTP(32)	0.32 (0.28)	1.26 (0.11)	3.21 (0.32)	7.45 (0.28)	3.36	1.00
GTP(33)	0.13 (0.22)	0.79 (0.21)	3.25 (0.28)	7.59 (0.27)	3.27	1.09
GTP(35)	0.23 (0.31)	1.17 (0.17)	3.69 (0.27)	8.34 (0.23)	3.26	1.02

[a]The number in parentheses refers to the position of 2-AP from the 5′-end.The pre-exponential factors (α_i) associated with each decay component (τ_i) as obtained by fitting the experimental points using eq 1 are given in parentheses; χ^2 values obtained from the data fitting algorithm are also listed. Errors are not mentioned explicitly to improve the clarity of presentation. Errors are ∼15% for τ_1 and α_1 and ∼10% for the other parameters.

Table 2. Parameters Associated with the Fluorescence Anisotropy Decay in the GTP-Binding RNA Aptamer

sample[a]	ϕ_1 (β_1)	ϕ_2 (β_2)	r_o[b]	r_{ss}[c]	χ^2
Without GTP: Rotational Correlation Times in ns (amplitude)					
GTP(4)	0.32 (0.58)	4.2 (0.42)	0.31	0.08	1.2
GTP(8)	0.46 (0.34)	5.8 (0.66)	0.31	0.10	1.1
GTP(32)	0.47 (0.45)	5.1 (0.55)	0.31	0.10	1.6
GTP(33)	0.54 (0.26)	6.1 (0.74)	0.31	0.13	1.6
GTP(35)	0.52 (0.44)	5.5 (0.56)	0.31	0.12	1.1
With GTP: Rotational Correlation Times in ns (amplitude)					
GTP(4)	0.23 (0.60)	3.0 (0.40)	0.31	0.10	1.2
GTP(8)	0.28 (0.35)	4.8 (0.65)	0.31	0.10	1.3
GTP(32)	0.36 (0.47)	4.0 (0.53)	0.31	0.08	1.2
GTP(33)	0.31 (0.27)	5.0 (0.73)	0.31	0.11	1.1
GTP(35)	0.45 (0.44)	4.6 (0.56)	0.31	0.11	1.2
With Urea (without GTP): Rotational Correlation Times in ns (amplitude)					
GTP(4)	0.54 (0.59)	4.0 (0.41)	0.31	0.09	1.2
GTP(8)	0.43 (0.46)	4.5 (0.54)	0.31	0.09	1.1
GTP(32)	0.45 (0.46)	4.0 (0.54)	0.31	0.09	1.2
GTP(33)	0.43 (0.27)	5.0 (0.73)	0.31	0.11	1.3
GTP(35)	0.45 (0.46)	4.2 (0.54)	0.31	0.09	1.2

[a]The number in parentheses refers to the position of 2-AP from the 5′-end. Errors are not mentioned explicitly to improve the clarity of presentation. Errors are ∼15% for φ_1 and β_1 and ∼10% for the other parameters. [b]r_0 is the initial anisotropy of 2-AP. The value of r_0 was kept constant at 0.31 in the analysis. [c]r_{ss} is the steady-state anisotropy, obtained by integration of the area under the time-resolved anisotropy decay curve.

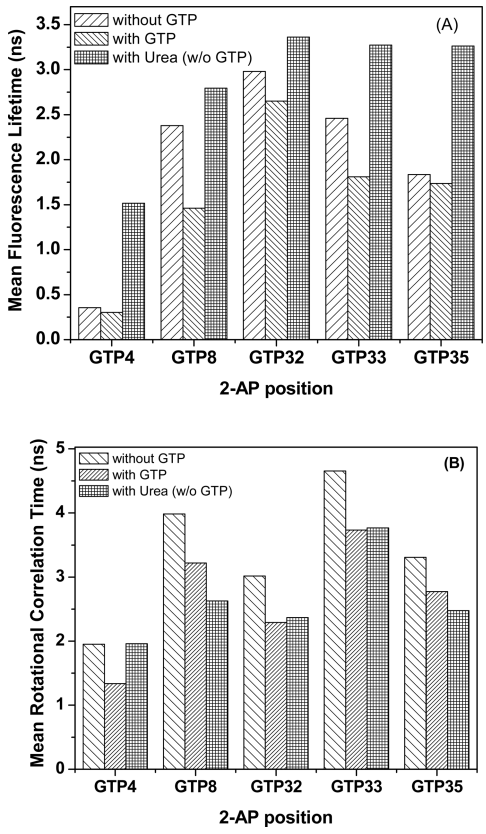

Figure 4. Site-specific dynamics in the GTP-binding RNA aptamer. 2-AP was incorporated at various locations of A in the RNA aptamer. The histograms show (A) mean fluorescence lifetimes and (B) mean rotational correlation times.

the complex. The position dependence of fluorescence intensity decay parameters (Table 2) shows that the shortest lifetime (τ_1) has a maximal contribution (∼80%) in GTP(4), resulting in the shortest value of τ_m compared to those for other locations studied in this work. The value of τ_1 and its amplitude have been used earlier as an effective signature of base pair formation,[46,47] and hence, the observed high amplitude is consistent with position 4 being in the stem region formed by Watson−Crick base pairs and A-form geometry.[14] Other observations of fluorescence decay kinetics are summarized as follows. (i) GTP binding caused site-specific changes in the decay kinetics at all the positions studied. However, the changes observed at positions 8 and 33 are larger compared to those observed at the other positions (Table 2 and Figure 4A). It is

dx.doi.org/10.1021/bi301110u | Biochemistry 2012, 51, 9260−9269

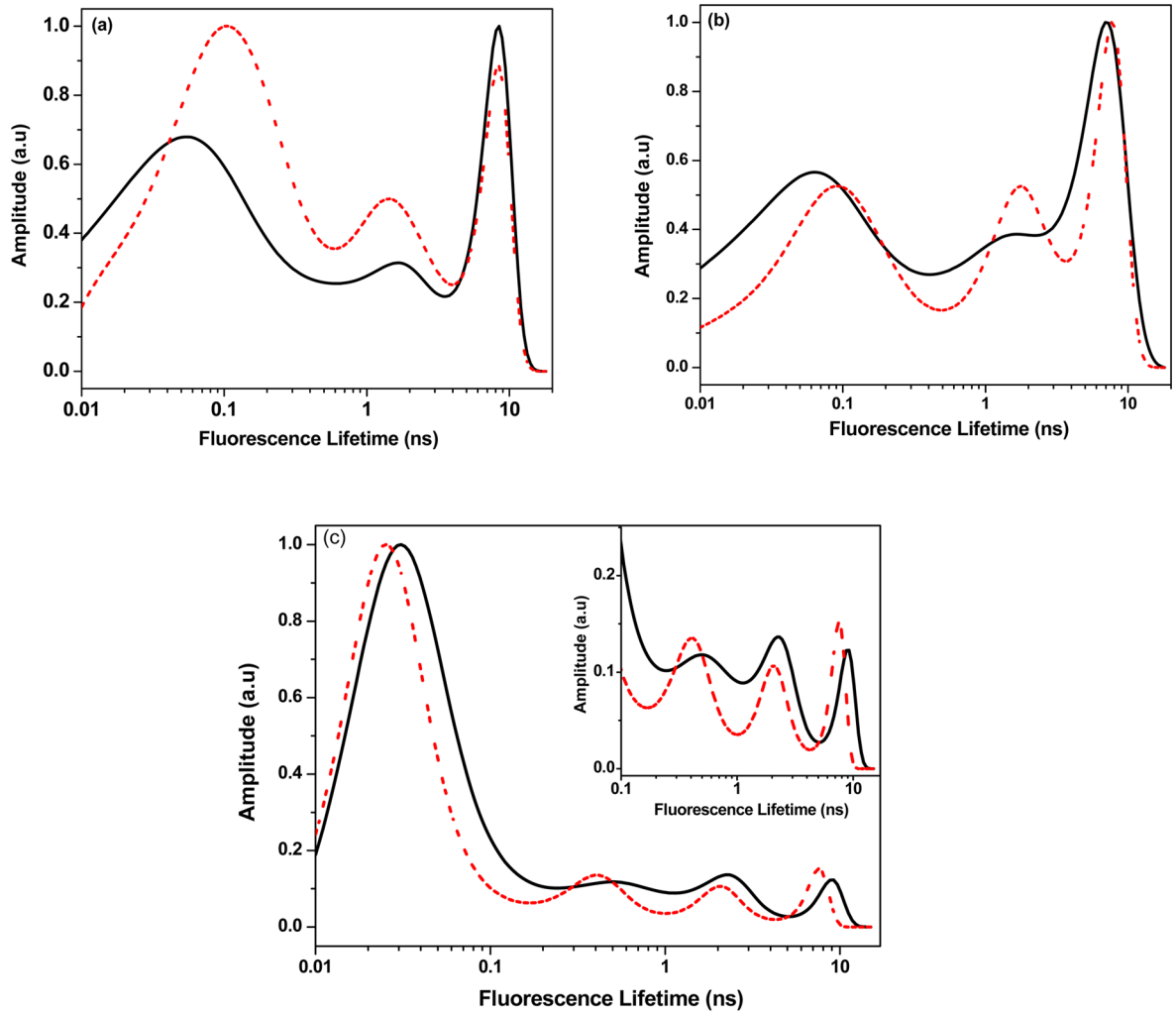

Figure 5. Fluorescence lifetime distribution (by the maximum entropy method) of 2-AP at different positions. Here, the lifetime distribution plots of position 8 (a), position 32 (b), and position 4 (c) in the presence (dashed line) and absence (solid line) of GTP are shown. The inset in panel c shows an expanded version of position 4 on the 0.1−10 ns scale.

interesting to note that these positions were identified as GTP-interacting bases from the NMR structure.[14] (ii) The larger value of τ_1 and hence the shorter value of τ_m at position 35 compared to those at positions 8, 32, and 33 could be the result of partial stacking of G12 with A35 inferred from NMR analysis.[14] (iii) Urea caused significant changes in the decay kinetics in all five positions studied, indicating structural loss in the aptamer that renders most of the observables largely independent of the location. (iv) The residual level of difference among the five positions, especially position 4, in the presence of urea could be due to residual structure and near-neighbor dependence on the fluorescence decay kinetics.

The fluorescence lifetime distribution estimated from the maximum entropy method (MEM) brings out, quantitatively, the level and nature of heterogeneity of the population in an unbiased manner.[54,69,70] MEM analysis of fluorescence decays revealed the presence of multimodal and heterogeneous populations of conformations of the aptamer (Figure 5). It is significant to note that the four lifetime values obtained from discrete analysis (Table 1) are clearly discernible as peaks of the distributions except for the shortest lifetime component (Figure 5). First, we note that the binding of GTP causes a reduction in the level of heterogeneity as demonstrated by the narrowing of distribution, resulting in the increase in the resolution of the distributions (Figure 5). This observation indicates that the binding of GTP makes the aptamer well-ordered and provides strong support for the conformational selection hypothesis, leading to "narrowing of conformer population" following ligand binding of RNA aptamers and switches, in general.[39,40,42] Second, the lifetime distribution profiles obtained for the free aptamer and the aptamer−GTP complex are very similar to each other despite the decrease in the widths of distributions caused by GTP binding. As noted above, this is clearly indicative of a preexisting aptamer structure similar to that of the complex, albeit with a higher level of heterogeneity, where a key tenet in the conformational selection model is experimentally validated by our data.

Site-Specific Motional Dynamics. Fluorescence anisotropy decay kinetics offers rich and direct information about the various dynamic modes such as the local or internal dynamics of the base, the segmental dynamics of the oligonucleotide backbone, and the global tumbling dynamics of the entire molecule.[46,52,70−73] While the first two modes reveal information about the internal dynamics of the molecular system, the last of the modes mentioned above provides information about the hydrodynamic size of the entire molecule.

dx.doi.org/10.1021/bi301110u | *Biochemistry* 2012, 51, 9260−9269

The fluorescence anisotropy decay of 2-AP in the free and GTP-bound aptamer could be fit satisfactorily to a sum of two exponentials (eq 5). The two rotational correlation times (ϕ) of 2-AP could be interpreted as being due to internal motion of the fluorophore with respect to the aptamer (ϕ_1) and a combination of segmental motion of the local region to which the 2-AP is linked and the global tumbling motion of the macromolecule (ϕ_2).[70] The validity of such an assignment for ϕ_2 is supported by (i) the significantly shorter value of ϕ_2 when compared to the global tumbling correlation time [8−10 ns (Figure 3)] obtained with PG (because the segmental dynamics could be faster than the global dynamics, the observed value of ϕ_2 is expected to be shorter than that of the global tumbling time) and (ii) the observed position dependence of ϕ_2 (Table 3). It should be noted that the global tumbling dynamics should be independent of the location and identity of the fluorophore while the segmental dynamics could be position-dependent. Furthermore, because PG becomes bound to nucleic acids rather rigidly,[58−60] its dynamics is mostly dominated by global tumbling dynamics of the nucleic acid unlike 2-AP, which reveals all the three modes of motional dynamics.[61−64,74,75]

Table 3. Bimolecular Quenching Rate Constants (k_q) for the GTP-Binding RNA Aptamer Determined Using the Stern−Volmer Equation

	k_q ($\times 10^9$ M^{-1} s^{-1})	
sample[a]	without GTP	with GTP
GTP(8)	6.8 ± 0.5	8.4 ± 0.6
GTP(32)	7.1 ± 0.4	7.9 ± 0.5
GTP(33)	4.1 ± 0.5	6.7 ± 0.4
GTP(35)	7.9 ± 0.8	7.1 ± 0.7

[a]The number in parentheses refers to the position of 2-AP from the 5′-end. GTP(4) did not yield reliable data presumably because of the very high amplitude of the shortest lifetime.

The values of the shorter correlation time (ϕ_1) obtained from the analysis were in the range of 0.2−0.5 ns, and the longer correlation time (ϕ_2) was in the range of 3−6 ns (Table 2). The values of the two correlation times and their amplitudes (β_1 and β_2) were dependent on the location of 2-AP in the free and GTP-bound form of the aptamer, again as expected for a structured oligonucleotide (Table 2). In the presence of urea, all four parameters are largely position-independent because of the loss of structure (Figure 4). The remaining low level of the nonflat profile seen in the presence urea could be due to residual structure that could persist even in the presence of urea. We also get a picture that the segmental dynamics that is revealed through ϕ_2 is not significantly altered by urea. Furthermore, a significantly larger amplitude associated with ϕ_1 for GTP(4) when compared to those of the other locations of 2-AP (Table 2) endows position 4 with special structural characteristics such as being in the double-stranded stem region as observed in DNA.[46,62] It has been observed in several cases that 2-AP situated in base-paired regions is associated with a larger amplitude of the shorter correlation time.[46,62,74,75] Although this counterintuitive observation has been interpreted as being due to large amplitude correlated motional dynamics of base-paired regions,[62] other mechanisms such as stacking-induced mixing of electronic states of 2-AP with those of adjacent bases resulting in tilting and fluctuations of the transition dipole moment axis[75] could not be ruled out. The latter mechanism is a result of electronic mixing in combination with motional dynamics. It is interesting to note that this special characteristic of position 4 is preserved in the GTP-bound form of the aptamer also (see below).

Binding of GTP resulted in a significant, albeit to different extents, reduction in the values of both correlation times. However, the amplitudes remained largely unchanged (Table 2). A decrease in ϕ_1 associated with 2-AP in polynucleotides indicates, in general, an increase in the level of structure. For example, the value of ϕ_1 was significantly smaller in double-stranded DNA than in single-stranded DNA.[46,62] Again, this could be due to the possible mechanisms mentioned above. The higher value of ϕ_1 observed at all the locations studied in the aptamer in the presence of urea that breaks the structure (Table 2) is consistent with this model. As mentioned above, the longer correlation time, ϕ_2, represents a combination of segmental and global motion of the aptamer. It is very likely that the observed GTP-induced shortening of ϕ_2 is largely due to GTP-induced compaction of the aptamer. This conclusion receives support from the observation of GTP-induced shortening of the tumbling correlation time seen with PG (Figure 3). In short, the site-specific fluorescence anisotropy decay kinetics shows that GTP binding results in an enhanced level of structure and compaction of the aptamer.

Lastly, we note that the pattern of the mean correlation time ($\phi_m = \sum \beta_i \phi_i$), which is a practical indicator of the overall dynamics, is very similar in the free aptamer and the aptamer−GTP complex (Figure 4B), similar to that of the mean lifetime (Figure 4A). Thus, our earlier conclusion about the general similarity of the structures of the free and GTP-bound aptamers is further strengthened.

Site-Specific Solvent Accessibility. The solvent accessibility of 2-AP at various locations in the aptamer was studied by dynamic fluorescence quenching experiments using acrylamide as the quencher (Q). The bimolecular quenching rate constant (k_q) was estimated from the linear plot of τ_0/τ versus [Q] using the Stern−Volmer equation. τ_0 and τ are the fluorescence lifetimes in the absence and presence of the quencher, respectively. Values of k_q estimated from these plots are listed in Table 3. We note that GTP binding results in an increase in the value of k_q in three of the four positions studied, indicating an enhanced level of solvent exposure of the nucleotides in the complex. Though the extents of GTP-induced changes are small, they are significant as the observation could be reproduced and beyond experimental errors. The observed increase in the value of k_q, which is a measure of dynamics leading to solvent exposure, is also consistent with the increase in the rate of motional dynamics caused by GTP binding (Table 2). In the context of the ordering of structure induced by GTP binding (see above), it seems likely that structure formation of the aptamer results in enhanced solvent exposure of bases in general. In the natural RNA riboswitches, such an exposure of bases could open up additional recognition events.

CONCLUSION

In conclusion, our work has shown that binding of GTP to the aptamer results in enhancement in the level of structural integrity of the aptamer as observed from changes in various fluorescence observables of 2-AP located at different sites. Furthermore, GTP binding leads to an increase in the level of compaction and stability of the aptamer, resulting in narrowing of the conformational heterogeneity of the aptamer. These observations support the conformational selection hypothesis of RNA switches in general. The main difference between

artificial RNA aptamers similar to the aptamer used in this work and the aptamer domains in naturally occurring RNA switches is the relatively smaller size of artificial aptamers. Although our work has pointed out several changes in the structure and dynamics of the aptamer following the binding of GTP, the changes are rather small in magnitude. The aptamer studied in this work is largely structured even in the absence of the ligand. Our results show that the free aptamer has structural features very similar to those of the complex but has large fluctuations around the final structure. This study tries to underscore the importance of the instrinsic structure of a ligand free aptamer that is further stabilized upon ligand binding. Similar conclusions have come from recent NMR studies of several riboswitch aptamer domains.[33,34] These recent studies point out that several riboswitch aptamer domains preorganize themselves into "bound" conformations in the absence of ligands,[33,34] a scenario leading to strengthening of the conformational selection theory of binding between a ligand and a macromolecule (GTP and aptamer, respectively, in this study).

Furthermore, we speculate here by taking a cue from the seminal studies published by Szostak and co-workers on GTP aptamers: a mere 10-fold tighter binding of GTP to an aptamer seems to require ∼10 additional "bits of information" in the structure that in a random sequence space leads to an ∼1000-fold decrease in its abundance.[76] Conformational narrowing rendered by a ligand (GTP in this case) in the structural space of an aptamer is perhaps a good intrinsic design that can offset such high "information costs".

It would be interesting to compare ligand-induced changes in such artificial and small aptamers with those in natural RNA switches that are known to undergo large changes in structure upon ligand binding.[28−40] Nevertheless, we believe that GTP-induced structural compaction and conformational selection in the RNA aptamer revealed in this study may serve as functionally relevant cues that the biology of a natural aptamer can make use of; this needs to be verified by additional experimentation.

AUTHOR INFORMATION

Corresponding Authors

*E-mail: gk@tifr.res.in (G.K.) or
*E-mail: bjrao@tifr.res.in (B.J.R.). Address: Homi Bhabha Road, Colaba, Mumbai 400 005, India. Phone: +91-22-2278-2301/2526. Fax: +91-22-2280-4610/4611.

Present Address

[§]Department of Chemistry, Assam University, Silchar 788 011, Assam, India.

Funding

This work was funded by the Tata Institute of Fundamental Research, Government of India. Both G.K. and B.J.R. acknowledge a J. C. Bose Grant (DST) that was useful in conducting this work.

Notes

The authors declare no competing financial interest.

ACKNOWLEDGMENTS

We thank Prof. N. Periasamy for the software used in the analysis of time-resolved fluorescence decays. We thank Ms. M. H. Kombrabail and Satya Narayan for assistance in the time-resolved fluorescence measurements.

ABBREVIATIONS

2-AP, 2-aminopurine; SELEX, systematic evolution of ligands by exponential enrichment; PG, PicoGreen; GTP, guanosine 5-triphosphate; TCSPC, time-correlated single-photon counting; MEM, maximum entropy method; IRF, instrument response function.

REFERENCES

(1) Hermann, T., and Patel, D. J. (2000) Adaptive Recognition by Nucleic Acid Aptamers. *Science 287*, 820−825.
(2) Carothers, J. M., Oestreich, S. C., and Szostak, J. W. (2006) Aptamers Selected for Higher-Affinity Binding Are Not More Specific for the Target Ligand. *J. Am. Chem. Soc. 128*, 7929−7937.
(3) Mayer, G. (2009) The Chemical Biology of Aptamers. *Angew. Chem., Int. Ed. 48*, 2672−2689.
(4) Ellington, A. D., and Szostak, J. W. (1990) *In vitro* selection of RNA molecules that bind specific ligands. *Nature 346*, 818−822.
(5) Tuerk, C., and Gold, L. (1990) Systematic evolution of ligands by exponential enrichment: RNA ligands to bacteriophage T4 DNA polymerase. *Science 249*, 505−510.
(6) Cho, E. J., Lee, J. W., and Ellington, A. D. (2009) Applications of Aptamers as Sensors. *Annu. Rev. Anal. Chem. 2*, 241−264.
(7) Famulok, M., and Mayer, G. (2011) Aptamer Modules as Sensors and Detectors. *Acc. Chem. Res. 44*, 1349−1358.
(8) Lise, J. N., Lars, F. O., and Veli, C. O. (2010) Aptamers Embedded in Polyacrylamide Nanoparticles: A Tool for in Vivo Metabolite Sensing. *ACS Nano 4*, 4361−4370.
(9) Lee, J. H., Mehmet, V. Y., Mazumdar, D., and Yi, L. (2010) Molecular diagnostic and drug delivery agents based on aptamer-nanomaterial conjugates. *Adv. Drug Delivery Rev. 62*, 592−605.
(10) Veli, C. O., and Schafer, T. (2011) Aptamer-Based Switchable Nanovalves for Stimuli-Responsive Drug Delivery. *Chem.—Eur. J. 17*, 9893−9896.
(11) Sefah, K., Phillips, J. A., Xiong, X. L., Meng, L., Van Simaeys, D., Chen, H., Martin, J., and Tan, W. H. (2009) Nucleic acid aptamers for biosensors and bio-analytical applications. *Analyst 134*, 1765−1775.
(12) Nutiu, R., and Li, Y. F. (2005) Aptamers with fluorescence-signaling properties. *Methods 37*, 16−25.
(13) Long, S. B., Long, M. B., White, R. R., and Sullenger, B. A. (2008) Crystal structure of an RNA aptamer bound to thrombin. *RNA 14*, 2504−2512.
(14) Carothers, J. M., Davis, J. H., Chou, J. J., and Szostak, J. W. (2006) Solution structure of an informationally complex high-affinity RNA aptamer to GTP. *RNA 12*, 567−579.
(15) Jenison, R. D., Gill, S. C., Pardi, A., and Polisky, B. (1994) High-resolution molecular discrimination by RNA. *Science 263*, 1425−1429.
(16) Zimmermann, G. R., Jenison, R. D., Wick, C. L., Simorre, J. P., and Pardi, A. (1997) Interlocking structural motifs mediate molecular discrimination by a theophylline-binding RNA. *Nat. Struct. Biol. 4*, 644−649.
(17) Fan, P., Suri, A. K., Fiala, R., Live, D., and Patel, D. J. (1996) Molecular Recognition in the FMN−RNA Aptamer Complex. *J. Mol. Biol. 258*, 480−500.
(18) Dieckmann, T., Butcher, S. E., Sassanfar, M., Szostak, J. W., and Feigon, J. (1997) Mutant ATP-binding RNA Aptamers Reveal the Structural Basis for Ligand Binding. *J. Mol. Biol. 273*, 467−478.
(19) Dieckmann, T., Suzuki, E., Nakamura, G. K., and Feigon, J. (1996) Solution structure of an ATP-binding RNA aptamer reveals a novel fold. *RNA 2*, 628−640.
(20) Kang, K. N., and Lee, Y. S. (2012) RNA Aptamers: A Review of Recent Trends and Applications. *Adv. Biochem. Eng. Biotechnol.*, DOI: 10.1007/10_2012_136 .
(21) Feigon, J., Dieckmann, T., and Smith, F. W. (1996) Aptamer structures from A to ζ. *Chem. Biol. 3*, 611−617.
(22) Patel, D. J., Suri, A. K., Jiang, F., Jiang, L., Fan, P., Kumar, R. A., and Nonin, S. (1997) Structure, Recognition and Adaptive Binding in RNA Aptamer Complexes. *J. Mol. Biol. 272*, 645−664.

(23) Ramos, A., Gubser, C. C., and Varani, G. (1997) Recent solution structures of RNA and its complexes with drugs, peptides and proteins. *Curr. Opin. Struct. Biol. 7*, 317−323.
(24) Yoshizawa, S., Fourmy, D., Eason, R. G., and Puglisi, J. D. (2002) Sequence-Specific Recognition of the Major Groove of RNA by Deoxystreptamine. *Biochemistry 41*, 6263−6270.
(25) Schneider, D., Gold, L., and Platt, T. (1993) Selective enrichment of RNA species for tight binding to *Escherichia coli* rho factor. *FASEB J. 7*, 201−207.
(26) Baugh, C., Grate, D., and Wilson, C. (2000) 2.8 Å Crystal Structure of the Malachite Green Aptamer. *J. Mol. Biol. 301*, 117−128.
(27) Sussman, D., Nix, J. C., and Wilson, C. (2000) The structural basis for molecular recognition by the vitamin B_{12} RNA aptamer. *Nat. Struct. Biol. 7*, 53−57.
(28) Stoddard, C. D., Montange, R. K., Hennelly, S. P., Rambo, R. P., Sanbonmatsu, K. Y., and Batey, R. T. (2010) Free State Conformational Sampling of the SAM-I Riboswitch Aptamer Domain. *Structure 18*, 787−797.
(29) Huang, L., Serganov, A., and Patel, D. J. (2010) Structural Insights into Ligand Recognition by a Sensing Domain of the Cooperative Glycine Riboswitch. *Mol. Cell 40*, 774−786.
(30) Jenkins, J. L., Krucinska, J., McCarty, R. M., Bandarian, V., and Wedekind, J. E. (2011) Comparison of a PreQ1 Riboswitch Aptamer in Metabolite-bound and Free States with Implications for Gene Regulation. *J. Biol. Chem. 286*, 24626−24637.
(31) Jiang, F., Kumar, R. A., Jones, R. A., and Patel, D. J. (1996) Structural basis of RNA folding and recognition in an AMP−RNA aptamer complex. *Nature 382*, 183−186.
(32) Bailor, M. H., Sun, X., and Al-Hashimi, H. M. (2010) Topology Links RNA Secondary Structure with Global Conformation, Dynamics, and Adaptation. *Science 327*, 202−206.
(33) Haller, A., Rieder, U., Aigner, M., Blanchard, S. C., and Micura, R. (2011) Conformational capture of the SAM-II riboswitch. *Nat. Chem. Biol. 7*, 393−400.
(34) Santner, T., Rieder, U., Kreutz, C., and Micura, R. (2012) Pseudoknot Preorganization of the $PreQ_1$ Class I Riboswitch. *J. Am. Chem. Soc. 134*, 11928−11931.
(35) Ferner, E.-D., Weigand, J. E., Ger, O. O., Schmidtke, S. R., Suess, B., and Wohnert, J. (2010) Highly Modular Structure and Ligand Binding by Conformational Capture in a Minimalistic Riboswitch. *Angew. Chem., Int. Ed. 49*, 6216−6219.
(36) Kloiber, K., Spitzer, R., Tollinger, M., Konrat, R., and Kreutz, C. (2011) Probing RNA dynamics via longitudinal exchange and CPMG relaxation dispersion NMR spectroscopy using a sensitive ^{13}C-methyl label. *Nucleic Acids Res. 39*, 4340−4351.
(37) Lee, M.-K., Gal, M., Frydmanb, L., and Varani, G. (2010) Real-time multidimensional NMR follows RNA folding with second resolution. *Proc. Natl. Acad. Sci. U.S.A. 107*, 9192−9197.
(38) Nix, J., Sussman, D., and Wilson, C. (2000) The 1.3 Å Crystal Structure of a Biotin-binding Pseudoknot and the Basis for RNA Molecular Recognition. *J. Mol. Biol. 296*, 1235−1244.
(39) Boehr, D. D., Nussinov, R., and Wright, P. E. (2009) The role of dynamic conformational ensembles in biomolecular recognition. *Nat. Chem. Biol. 5*, 789−796.
(40) Haller, A., Soulière, M. F., and Micura, R. (2011) The Dynamic Nature of RNA as Key to Understanding Riboswitch Mechanisms. *Acc. Chem. Res. 44*, 1339−1348.
(41) Montange, R. K., and Batey, R. T. (2008) Riboswitches: Emerging Themes in RNA Structure and Function. *Annu. Rev. Biophys. 37*, 117−133.
(42) Nahvi, A., Sudarsan, N., Ebert, M. S., Zou, X., Brown, K. L., and Breaker, R. R. (2002) Genetic Control by a Metabolite Binding mRNA. *Chem. Biol. 9*, 1043−1049.
(43) Sowers, L. C., Fazakerley, G. V., Eritja, R., Kaplan, B. E., and Goodman, M. F. (1986) Base pairing and mutagenesis: Observation of a protonated base pair between 2-aminopurine and cytosine in an oligonucleotide by proton NMR. *Proc. Natl. Acad. Sci. U.S.A. 83*, 5434−5438.
(44) Jean, J. M., and Hall, K. B. (2002) 2-Aminopurine Electronic Structure and Fluorescence Properties in DNA. *Biochemistry 41*, 13152−13161.
(45) Seibert, E., Ross, J. B., and Osman, R. (2002) Role of DNA Flexibility in Sequence-Dependent Activity of Uracil DNA Glycosylase. *Biochemistry 41*, 10976−10984.
(46) Ramreddy, T., Sen, S., Rao, B. J., and Krishnamoorthy, G. (2003) DNA Dynamics in RecA DNA Filaments: ATP Hydrolysis-Related Flexibility in DNA. *Biochemistry 42*, 12085−12094.
(47) Hochstrasser, R. A., Carver, T. E., Sowers, L. C., and Millar, D. P. (1994) Melting of a DNA Helix Terminus within the Active Site of a DNA Polymerase. *Biochemistry 33*, 11971−11979.
(48) Nordlund, T. M., Andersson, S., Nilsson, L., Rigler, R., Graslund, A., and McLaughlin, L. W. (1989) Structure and dynamics of a fluorescent DNA oligomer containing the EcoRI recognition sequence: Fluorescence, molecular dynamics, and NMR studies. *Biochemistry 28*, 9095−9103.
(49) Wan, C., Fiebig, T., Schiemann, O., Barton, J. K., and Zewail, A. H. (2000) Femtosecond direct observation of charge transfer between bases in DNA. *Proc. Natl. Acad. Sci. U.S.A. 97*, 14052−14055.
(50) Thomas, T., Phillip, D. Z., Ruth, L., David, P. B., and Phillip, A. S. (1999) Targeted mRNA degradation by double-stranded RNA in vitro. *Genes Dev. 13*, 3191−3197.
(51) Bevington, P. R. (1969) *Data Reduction and Error Analysis for the Physical Sciences*, McGraw-Hill, Inc., New York.
(52) Lakowicz, J. R. (2000) *Principles of Fluorescence Spectroscopy*, 2nd ed., Kluwer Academic/Plenum Publishers, New York.
(53) Brochon, J. C. (1994) Maximum entropy method of data analysis in time-resolved spectroscopy. *Methods Enzymol. 240*, 262−311.
(54) Swaminathan, R., and Periasamy, N. (1996) Analysis of fluorescence decay by the maximum entropy method: Influence of noise and analysis parameters on the width of the distribution of lifetimes. *Proc. Indian Acad. Sci., Chem. Sci. 108*, 39−49.
(55) Huang, F., Lerner, E., Sato, S., Amir, D., Haas, E., and Fersht, A. R. (2009) Time-Resolved Fluorescence Resonance Energy Transfer Study Shows a Compact Denatured State of the B Domain of Protein A. *Biochemistry 48*, 3468−3476.
(56) Puglisi, J. D., and Tinoco, I., Jr. (1989) Absorbance melting curve of RNAs. *Methods Enzymol. 180*, 304−325.
(57) Jose, D., Datta, K., Johnson, N. P., and Von Hippel, P. H. (2009) Spectroscopic Studies of position-specific DNA "breathing" fluctuations at replication forks and primer-template junctions. *Proc. Natl. Acad. Sci. U.S.A. 106*, 4231−4236.
(58) Noothi, S. K., Kombrabail, M., Kundu, T. K., Krishnamoorthy, G., and Rao, B. J. (2009) Enhanced DNA dynamics due to cationic reagents, topological states of dsDNA and high mobility group box 1 as probed by PicoGreen. *FEBS J. 276*, 541−551.
(59) Noothi, S. K., Kombrabail, M., Rao, B. J., and Krishnamoorthy, G. (2010) Fluorescence characterization of the structural heterogeneity of polytene chromosomes. *J. Fluoresc. 20*, 37−41.
(60) Dragan, A. I., Casas-Finet, J. R., Bishop, E. S., Strouse, R. J., Schenerman, M. A., and Geddes, C. D. (2010) Characterization of PicoGreen Interaction with dsDNA and the Origin of Its Fluorescence Enhancement upon Binding. *Biophys. J. 99*, 3010−3019.
(61) Nag, N., Rao, B. J., and Krishnamoorthy, G. (2007) Altered Dynamics of DNA Bases Adjacent to a Mismatch: A Cue for Mismatch Recognition by MutS. *J. Mol. Biol. 374*, 39−53.
(62) Ramreddy, T., Rao, B. J., and Krishnamoorthy, G. (2007) Site-Specific Dynamics of Strands in ss- and ds-DNA As Revealed by Time-Domain Fluorescence of 2-Aminopurine. *J. Phys. Chem. B 111*, 5757−5766.
(63) Ramreddy, T., Kombrabail, M., Krishnamoorthy, G., and Rao, B. J. (2009) Site-Specific Dynamics in TAT Triplex DNA As Revealed by Time-Domain Fluorescence of 2-Aminopurine. *J. Phys. Chem. B 113*, 6840−6846.
(64) Goel, T., Mukherjee, T., Rao, B. J., and Krishnamoorthy, G. (2010) Fluorescence Dynamics of Double- and Single-Stranded DNA

Bound to Histone and Micellar Surfaces. *J. Phys. Chem. B 114*, 8986−8993.
(65) Rachofsky, E. L., Osman, R., and Ross, J. B. (2001) Probing Structure and Dynamics of DNA with 2-Aminopurine: Effects of Local Environment on Fluorescence. *Biochemistry 40*, 946−956.
(66) Guest, C. R., Hochstrasser, R. A., Sowers, L. C., and Millar, D. P. (1991) Dynamics of Mismatched Base Pairs in DNA. *Biochemistry 30*, 3271−3279.
(67) Ward, D. C., Reich, E., and Stryer, L. (1969) Fluorescence Studies of Nucleotides and Polynucleotides. *J. Biol. Chem. 244*, 1228−1237.
(68) Thomas, L., Eleanor, Y. M. B., Goran, P., Robert, K. N., David, T. F. D., Axel, J. S., Anita, C. J., and Elmar, W. (2007) 2-Aminopurine Flipped into the Active Site of the Adenine-Specific DNA Methyltransferase M.TaqI: Crystal Structures and Time-Resolved Fluorescence. *J. Am. Chem. Soc. 129*, 6240−6248.
(69) Sarkar, S. S., Udgaonkar, J. B., and Krishnamoorthy, G. (2011) Reduced Fluorescence Lifetime Heterogeneity of 5-Fluorotryptophan in Comparison to Tryptophan in Proteins: Implication for Resonance Energy Transfer Experiments. *J. Phys. Chem. B 115*, 7479−7486.
(70) Krishnamoorthy, G. (2012) Motional dynamics in proteins and nucleic acids control their function: Revelation by time-domain fluorescence. *Curr. Sci. 102*, 266−276.
(71) Lakshmikanth, G. S., and Krishnamoorthy, G. (1999) Solvent-Exposed Tryptophans Probe the Dynamics at Protein Surfaces. *Biophys. J. 77*, 1100−1106.
(72) Saxena, A. M., Udgaonkar, J. B., and Krishnamoorthy, G. (2006) Characterization of Intra-molecular Distances and Site-specific Dynamics in Chemically Unfolded Barstar: Evidence for Denaturant-dependent Non-random Structure. *J. Mol. Biol. 359*, 174−189.
(73) Mukhopadhyay, S., Nayak, P. K., Udgaonkar, J. B., and Krishnamoorthy, G. (2006) Characterization of the Formation of Amyloid Protofibrils from Barstar by Mapping Residue-specific Fluorescence Dynamics. *J. Mol. Biol. 358*, 935−942.
(74) Larsen, O. F. A., Ivo, H. M., Stokkum, V., Gobets, B., Grondelle, R. V., and Amerongen, H. V. (2001) Probing the Structure and Dynamics of a DNA Hairpin by Ultrafast Quenching and Fluorescence Depolarization. *Biophys. J. 81*, 1115−1126.
(75) Hall, K. B., and Williams, D. J. (2004) Dynamics of the IRE RNA hairpin loop probed by 2-aminopurine fluorescence and stochastic dynamics simulations. *RNA 10*, 34−47.
(76) Carothers, J. M., Oestreich, S. C., Davis, J. H., and Szostak, J. W. (2004) Informational Complexity and Functional Activity of RNA Structures. *J. Am. Chem. Soc. 126*, 5130−5137.